Intense mixing of the Faroe Bank Channel overflow

Ilker Fer,[1,2] Gunnar Voet,[3] Knut S. Seim,[4] Bert Rudels,[5,6] and Katrin Latarius[3]

Received 25 November 2009; revised 29 December 2009; accepted 5 January 2010; published 29 January 2010.

[1] The continuous, swift flow of cold water across the sill of the Faroe Bank Channel, the deepest passage from the Nordic Seas to the North Atlantic Ocean, forms a bottom-attached dense plume (overflow). The amount and distribution of entrainment and mixing that the overflow encounters during its descent influence the ventilation of the deep North Atlantic, however, remain poorly known due to lack of direct measurements. Using the first direct turbulence measurements, we describe the dynamic properties and mixing of the overflow plume as it descends toward the Iceland Basin. The vigorously turbulent plume is associated with intense mixing and enhanced turbulent dissipation near the bottom and at the plume-ambient interface, but with a quiescent core. Our measurements show a pronounced transverse circulation consistent with rotating plume dynamics, a strong lateral variability in entrainment velocity, and a vertical structure composed of order 100 m thick stratified interface and comparably thick well-mixed bottom boundary layer with significant transport and entrainment. **Citation:** Fer, I., G. Voet, K. S. Seim, B. Rudels, and K. Latarius (2010), Intense mixing of the Faroe Bank Channel overflow, *Geophys. Res. Lett.*, *37*, L02604, doi:10.1029/2009GL041924.

1. Introduction

[2] The export of cold, dense water from the Norwegian Sea through the Faroe Bank Channel (FBC, Figure 1) into the sub-polar North Atlantic accounts for about one third of the total overflow from the Nordic Seas [*Hansen and Østerhus*, 2007]. The FBC overflow, a bottom-attached gravity current, descends the sloping topography under the combined influence of pressure gradient, bottom friction and the Earth's rotation, and mixes with overlying water [*Saunders*, 2001; *Mauritzen et al.*, 2005]. The latter determines the end-product properties associated with the source water and needs to be properly represented in climate models for credible climate projections [*Legg et al.*, 2009]. Despite the importance of mixing of the FBC overflow, no previous measurements of turbulence have been available. Motivated by this lack of measurements we conducted such a survey in June 2008.

2. Measurements and Data

[3] The obtained data set includes vertical profiles of hydrography and velocity from 63 casts with a conductivity-temperature-depth (CTD, SBE911+) package equipped with down and uplooking lowered acoustic Doppler current profilers (LADCPs, 300 kHz Workhorse), and of turbulence profiles from 90 casts with a vertical microstructure profiler (VMP, Rockland Sci. Int.). The VMP is equipped with accurate CTD sensors and a pair of microstructure shear probes used for measuring the dissipation rate of turbulent kinetic energy (ε). Turbulent shear is sampled at 512 Hz at a profiling speed of 0.6 m s^{-1}. Stations are occupied along the path of the overflow plume and along six sections starting from the sill crest (section A) to about 120 km downstream (section F, Figure 1a).

3. Technical Details

3.1 Currents, Dissipation Rate, and Eddy Diffusivity

[4] The velocity profile is calculated as 4 m vertical averages using the inverse method [*Visbeck*, 2002] constrained by accurate shipboard navigation and bottom tracking by the LADCP, and detided using a barotropic tidal model [*Egbert et al.*, 1994] for the European Shelf at 1/30° resolution. Tidal velocity is within 3 to 34% (18% on the average) of the maximum velocity at a given station.

[5] The profiles of ε are produced as 1 m vertical averages to a noise level of 10^{-10} W kg^{-1} [*Fer*, 2006]. The diapycnal eddy diffusivity is calculated using three different formulations: First, an upper limit is obtained from $K_\rho = 0.2\varepsilon N^{-2}$ [*Osborn*, 1980] assuming 17% mixing efficiency. $N = [-g/\rho(\partial\rho/\partial z)]^{1/2}$ is the buoyancy frequency, g is the gravitational acceleration, and ρ is density. Second, we use $K_\rho = 2\nu(\varepsilon / \nu N^2)^{1/2}$ [*Shih et al.*, 2005], suggested for $\varepsilon / \nu N^2 > 100$, valid for our data ($\nu$ is the viscosity). This formulation, inferred from direct numerical simulation results, has been supported by field data [*Fer and Widell*, 2007]. Third, we use a gradient Richardson number (Ri) dependent mixing efficiency with the range of parameters validated against microstructure measurements [*Peters and Baumert*, 2007]. $\mathrm{Ri} = N^2/S^2$, where S is the shear. In all calculations, N is inferred from 4 m vertical gradients of sorted σ_θ (potential density referenced to nil pressure) profiles. The vertical scale is chosen to be consistent with shear calculations and the sorting approximates the background stratification against which the turbulence works.

3.2 Plume Properties and Stress

[6] The density anomaly, ρ', is obtained as deviations from an exponential background σ_θ profile fitted to observations excluding the plume. Velocity profiles are rotated into streamwise (u) and transverse (v, positive to the right of u) components with respect to the direction of the maximum

[1]Geophysical Institute, University of Bergen, Bergen, Norway.
[2]Bjerknes Centre for Climate Research, Bergen, Norway.
[3]Institute of Oceanography, University of Hamburg, Hamburg, Germany.
[4]Department of Marine Technology, Norwegian University of Science and Technology, Trondheim, Norway.
[5]Department of Physics, University of Helsinki, Helsinki, Finland.
[6]Finnish Meteorological Institute, Helsinki, Finland.

0094-8276/10/2009GL041924$05.00

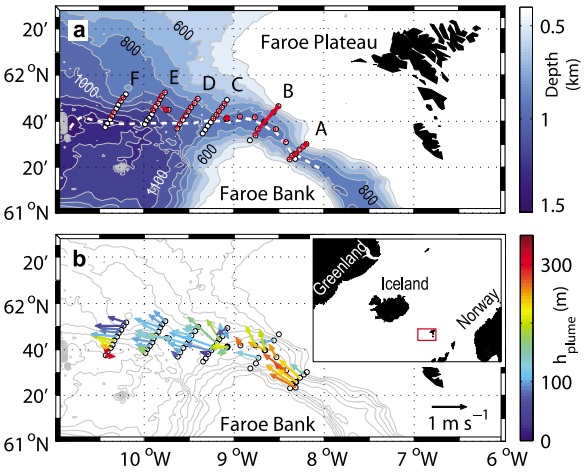

Figure 1. (a) Bathymetric contours drawn at 100 m intervals starting with 400 m, together with the thalweg (deepest point of the channel, white dashed line), sampling stations (CTD-LADCP, circles, and VMP, red crosses) and sections A to F. (b) Overflow velocity (arrows) averaged over h_{plume} (color). The salient features of the plume velocity and thickness are described in section 4. The inset shows the experiment location (red).

velocity (u_{nose}) in the bottom 200 m. The depth of the plume interface z_i and plume thickness h_{plume} are inferred from the $\sigma_\theta = 27.65$ kg m^{-3} isopycnal [*Mauritzen et al.*, 2005; *Girton et al.*, 2006]. The well-mixed bottom layer (BL) thickness is estimated as the height above bottom (HAB) where the density difference from the bottommost value exceeds 0.01 kg m^{-3}. The stratified interfacial layer (IL) is defined as the layer between the top of BL and the depth above the interface where $\partial\sigma_\theta/\partial z$ first drops below 5×10^{-4} kg m^{-4}. These thresholds robustly delineate the BL and IL. The calculation of integral plume properties and density-anomaly-weighted averages follows *Girton and Sanford* [2003]. The internal Froude number is calculated in two ways: from integral plume properties of each section using $\mathrm{Fr} = U/\sqrt{g'H}$ and using a two-layer formulation devised for transverse variations in velocity [*Pratt*, 2008]. In the former method g' is the reduced gravity, $H = A/(2W_{0.5})$ is the mean plume thickness for a section with area A and plume "half-width" $W_{0.5}$ [*Girton and Sanford*, 2003], and $U = Q_p/A$, using the section-integrated plume volume transport Q_p.

[7] The bottom shear stress, $\tau_{\mathrm{b}} = \rho u_*^2$, is estimated using the friction velocity u_* from the slope of a linear fit of u against the log of HAB, assuming law of the wall (LOW). A series of fits is made for each profile, starting with 3 data points (12 m) and increasing to a maximum of BL thickness. The value with the least error, inferred from goodness of the fit, is chosen for analysis. The Ekman number $\mathrm{Ek} = u_*^2 / fuh_{plume}$ and the drag coefficient $\mathrm{C_D} = u_*^2 / u_{nose}^2$ are obtained. Stress at the plume-ambient interface is estimated assuming a balance between the shear production, the dissipation rate, and the resulting buoyancy flux ($0.2\bar{\varepsilon}$), as $\tau_i = 1.2\bar{\varepsilon}/\overline{(\rho du/dz)}$, where overbars denote averaging over the interface thickness.

4. Results and Discussion

[8] The overflow plume descends the channel and the slope of the Iceland-Faroe Ridge with a typical speed of 0.5 – 1 m s^{-1}, reaching a maximum velocity of 1.35 m s^{-1} at section C (Figure 1b). Plume thickness averaged over stations is $h_{\mathrm{plume}} = 160 \pm 70$ m ($\pm$ 1 standard deviation, σ). Mean overflow thickness (H) inferred from section-integrated properties is between 110 m (section E) and 350 m (section B). All sections, however, show significant lateral variability (Figure 2).

[9] The vertical structure of the overflow is composed of a 70 ± 35 m thick well-mixed BL, overlaid by a 120 ± 60 m thick IL. With the caveat that the section-averaged transports are not synoptic with respect to variability on tidal and subtidal scales [*Geyer et al.*, 2006], the overflow is about equally distributed between the BL (0.9 ± 0.1 Sv, 1 Sv $\equiv 10^6$ m^3 s^{-1}) and the IL (1 ± 0.3 Sv). The presence of a thick IL was also observed at the Red Sea [*Peters et al.*, 2005], the Denmark Strait [*Girton and Sanford*, 2003], and the Mediterranean

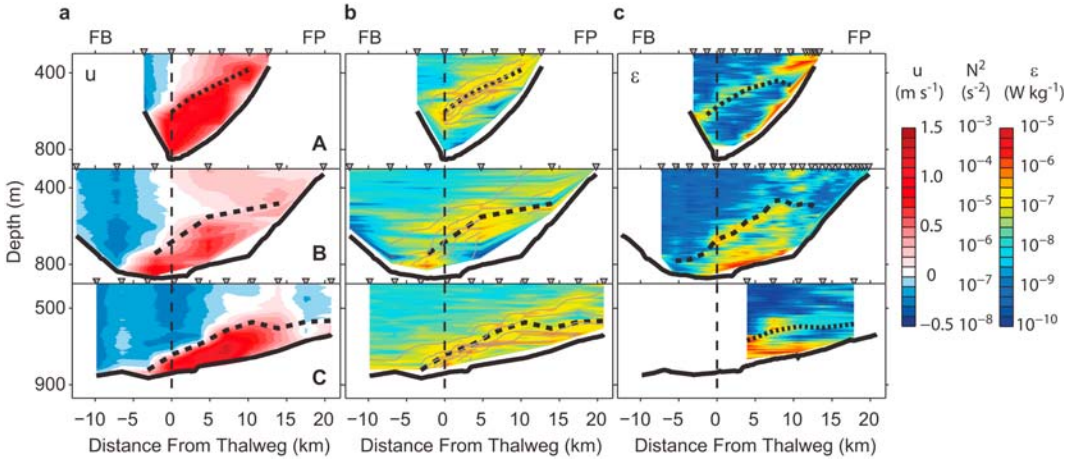

Figure 2. Contours of (a) downchannel velocity, u, (b) stratification, N^2 (color), and σ_θ at 0.1 kg m^{-3} intervals (gray), and (c) dissipation rate, ε, for sections A to C. Locations of the stations (triangles), the Faroe Bank (FB), and the Faroe Plateau (FP) are indicated. Dashed curves delineate the plume interface ($\sigma_\theta = 27.65$ kg m^{-3}).

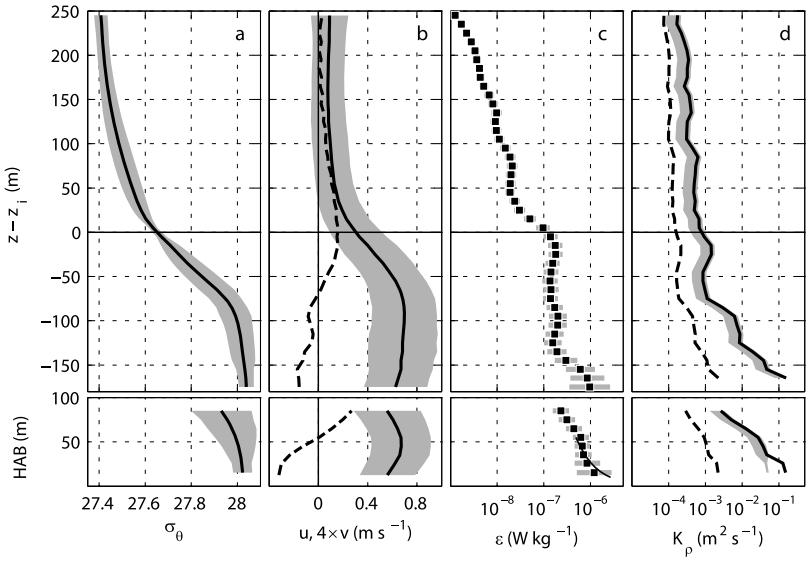

Figure 3. Survey averaged profiles of (a) σ_θ (± 1σ, gray shading), (b) downchannel, u (solid line, ±1σ, gray shading), and cross-channel, v (dashed line, multiplied by 4 for clarity), component of the velocity, (c) dissipation rate, ε (95% confidence limits, gray bars), and (d) eddy diffusivity, K_ρ, using *Osborn* [1980] (solid line), *Peters and Baumert* [2007] (gray), and *Shih et al.* [2005] (dashed line). Profiles are averaged in 10-m vertical bins referenced to (top) the interface depth, z_i, and to (bottom) bottom (HAB). Thin line in Figure 3c (bottom) is fit to LOW ($\varepsilon = u_*^3 / 0.4z$) in the bottom 55 m yielding u_* = 2.2 cm s^{-1} (τ_b = 0.5 Pa).

[*Price et al.*, 1993] outflow plumes, and suggests that bulk parameterization of entrainment [*Legg et al.*, 2009] devised for gravity currents with relatively thin interface may not be adequate.

[10] The velocity maximum is typically located deeper than the interface and is associated with weak ε as a result of weak shear production of turbulent kinetic energy (see the quiescent core at section A, Figure 2). This quiescent layer is present at all sections. The average thickness of layer with $\varepsilon < 10^{-8}$ W kg^{-1} below the interface is 40 m for the core stations and varies between 15 m (section B) and 60 m (section A). In the BL and the IL ε is exceptionally large, reaching 10^{-5} W kg^{-1} (Figure 2c). Typically BL is 20–70 m thicker than the bottom layer with enhanced dissipation. The vigorous turbulence near the bottom is due to stirring by the bottom shear stress. Enhanced mixing at the stratified and highly-sheared IL where Ri < 1 can be due to coexisting shear instabilities and internal wave-turbulence transition [*Baumert and Peters*, 2009] and vertical transport of turbulence [*Umlauf*, 2009]. The internal structure of turbulence in the FBC overflow is reminiscent of the observations in the Baltic Sea [*Umlauf et al.*, 2007], particularly the quiescent central region, and the asymmetry in ε at the sill section with enhanced ε where the interface intersects the Faroe Plateau slope (Figure 2b). A wedge-shaped interface, related to the secondary flow in the IL, as discussed by *Umlauf and Arneborg* [2009], is not resolved in our data set.

[11] Survey-averaged profiles are constructed for plume stations in 10-m thick bins relative to the interface and relative to the bottom (Figure 3). Due to variable interface depth and plume thickness, the average profiles cannot be combined (i.e., the lower part of Figure 3 (top) will not be consistent with Figure 3 (bottom) due to averaging). Dissipation rates, exceeding 10^{-7} W kg^{-1} in the plume, increase by one order of magnitude as the bottom is approached, consistent with LOW (thin line in Figure 3c). The mixing efficiency implied by the models of *Shih et al.* [2005] and *Peters and Baumert* [2007] differ significantly, particularly in weakly stratified layers (Figure 3d). The shear is strong throughout the IL, but the maximum in ε apparent in Figure 2c near the interface is smoothed out as a result of averaging. When calculated using the density and velocity profiles in Figure 3, Ri < 1 between 20 m above and 40 m below the interface, with a minimum value of 0.6 at 15 m below the interface. Ri < 1 in the entire BL with Ri < 0.25 in the bottommost 25 m. Low Ri in the BL is due to a combination of weak stratification and mean shear of the logarithmic velocity profile, whereas that in the IL is due to strong shear across the strongly stratified interface. Previous observations from a mooring near the FBC sill show frequent occurrence of low Ri in the IL, modulated by tidal and inertial flows [*Saunders*, 2001].

[12] The transverse velocity, v (Figure 3b), has a vertical structure consistent with the rotating gravity current dynamics [*Umlauf and Arneborg*, 2009]. Water in the IL is transported to the right, looking downstream (a transverse geostrophic transport due to the downchannel tilt of the plume interface), and water in the BL is transported to the left, consistent with an Ekman bottom boundary layer, leading to a flattening and broadening of the plume. Integrated across the IL and BL, the transverse flow approximately balances with 5 m^2 s^{-1} in the IL, −3.3 m^2 s^{-1} in the BL (−4.5 m^2 s^{-1} if an unresolved 15-m thick bottom layer with v = −8 cm s^{-1}, the bottommost average value, is included).

[13] The FBC overflow can be characterized by Fr between 0.5 and 1 and by Ek between 0.05 and 0.2; that is, the plume is thicker than the frictional boundary layer (Figure 4). In contrast to the Red Sea outflow [*Peters et al.*, 2005], the FBC overflow is significantly diluted in the BL. The buoy-

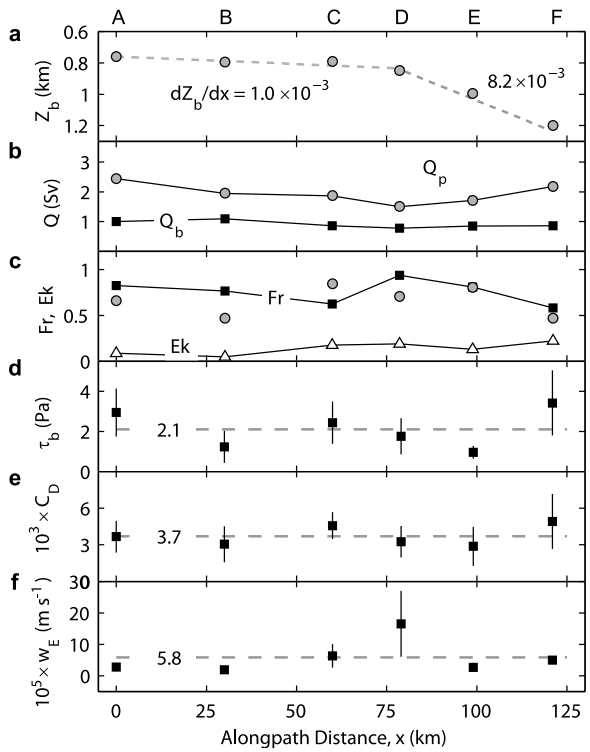

Figure 4. Downstream evolution of section-averaged properties. (a) Mass-anomaly-weighted depth of the plume, Z_b [*Girton and Sanford*, 2003]. Linear fits between sections A-D and D-F yield a descent rate of 1 m and 8.2 m per km along the path, respectively (dashed lines). (b) Volume transport in the overflow plume (Q_p, circles) and in the BL (Q_b, squares). (c) Froude number (Fr, following *Pratt* [2008], squares; and using section integral properties, circles), and Ekman number, Ek (triangles). (d) Bottom stress, τ_b, and (e) drag coefficient, C_D, from LADCP profiles, and (f) the entrainment velocity, w_E, from ε [*Arneborg et al.*, 2007]. The survey-averaged values are indicated by dashed lines. Error bars are $\sigma_e = \sigma\sqrt{n-1}$, where σ is the standard deviation and n is the number of plume stations in a section.

ancy averaged in BL (IL) increases by 1.4×10^{-3} m s^{-2} (5×10^{-4} m s^{-2}) on the first 80 km. This suggests entrainment into the BL, through, e.g., internal mixing in the plume, entrainment as a result of the transverse circulation, or lateral entrainment due to stirring by mesoscale eddies. The volume transport, however, is nearly constant in the BL (Q_b in Figure 4b), counterintuitive to the expected increase due to entrainment. Detrainment [*Baines*, 2005] might explain the lack of increase in Q_b. Nevertheless, interpreted together with the Red Sea outflow observations which show a similar vertical density structure but no dilution in BL, we suggest that the transverse circulation supplying the warmer interface water into the Ekman layer may cause the dilution in the BL. Q_b remains nearly constant due to the approximate lateral balance of the transverse circulation; that is, water entrained in the BL is transported back to the IL.

[14] Section-averaged K_ρ varies between $(2 - 10) \times 10^{-4}$ m^2 s^{-1} in the IL and between $(10 - 320) \times 10^{-4}$ m^2 s^{-1} in the BL, consistent with heat-budget considerations [*Saunders*, 1990; *Duncan et al.*, 2003]. The entrainment velocity, w_E, calculated from ε [*Arneborg et al.*, 2007] (assuming 17% mixing efficiency) varies by one order of magnitude laterally in each section (except section F). Section-averaged w_E increases fivefold from 3×10^{-5} m s^{-1} at the sill to 1.7×10^{-4} m s^{-1} at section D (Figure 4f) where Fr is accordingly at its highest, close to unity. The entrainment parameter, w_E/U, increases by one order of magnitude from 3.8×10^{-5} to 3.3×10^{-4}. The largest mixing and entrainment rates are observed at section D in the vicinity of the hot-spot of mixing identified by *Mauritzen et al.* [2005]. Detailed analysis of earlier observations suggests that FBC overflow is hydraulically controlled [*Girton et al.*, 2006] with the critical section (i.e., Fr = 1) located between 20 – 90 km down sill, comparing well with Fr $\approx$ 1 at our section D. While the overflow volume transport, Q_p, increases downstream of section D (consistent with enhanced entrainment), Q_p decreases between sections A and D. The mesoscale variability of the overflow makes the comparison of single sections complex.

[15] The overflow plume descends the slope as a result of bottom friction. The descent rate is relatively small between sections A-D and increases farther downstream (Figure 4a), comparable to that of the Denmark Strait plume [*Girton and Sanford*, 2003], but significantly larger than 2.5 m km^{-1} predicted by *Killworth* [2001]. The bottom stress $\tau_b = 2.1 \pm 0.4$ Pa, corresponding to a drag coefficient of $C_D = (3.7 \pm 0.4) \times 10^{-3}$, is large throughout the channel, and in the range of previous observations [*Mauritzen et al.*, 2005]. When tides are included, the survey-mean C_D increases by 20%. The average bottom stress inferred from the velocity profiles is about four times larger than that estimated from ε measurements near the bottom (Figure 3c), similar to observations from diverse sites and can be attributed to, e.g., the form drag. The stress at the IL is relatively weak, $\tau_i = 0.05 \pm 0.02$ Pa. Inferred from the balance of buoyancy, total drag (due to τ_b and τ_i) and Coriolis force acting on a slab of plume [*Girton and Sanford*, 2003], the total stress to account for the observed descent rates is 0.9 (sections A-D) and 4.9 Pa (D-F). Recalling that $\tau_b \approx \tau_b + \tau_i$ in our data set, Figure 4d does not show this trend, suggesting that the observed descent rates cannot be described by this simple force balance.

5. Concluding Remarks

[16] Our observations reveal the anatomy and mixing processes of the FBC overflow plume and add to our understanding of a highly sheared and stratified gravity current in a rotating system. The overflow plume is characterized by strong lateral variability in entrainment and mixing with a significant vertical structure including an about 100 m thick strongly-stratified interfacial layer. A transverse circulation actively dilutes the bottom layer of the plume. Neither the bulk entrainment parameterizations, mainly devised for non-rotating, two-layer gravity current plume dynamics, nor the traditional turbulence closure models will be adequate in representing mixing of the dense overflow plume downstream of the FBC sill.

[17] **Acknowledgments.** This study is funded by the Research Council of Norway, through Bipolar Atlantic Thermohaline Circulation (BIAC) project. Comments from an anonymous reviewer, L. Umlauf, H. Peters,

H. Z. Baumert, and T. Özgökmen are greatly appreciated. This is publication no. A 271 from the Bjerknes Centre for Climate Research.

References

Arneborg, L., V. Fiekas, L. Umlauf, and H. Burchard (2007), Gravity current dynamics and entrainment: A process study based on observations in the Arkona Basin, *J. Phys. Oceanogr.*, *37*, 2094–2113, doi:10.1175/JPO3110.1.

Baines, P. G. (2005), Mixing regimes for the flow of dense fluid down slopes into stratified environments, *J. Fluid Mech.*, *538*, 245–267, doi:10.1017/S0022112005005434.

Baumert, H. Z., and H. Peters (2009), Turbulence closure: Turbulence, waves and the wave-turbulence transition—Part 1: Vanishing mean shear, *Ocean Sci.*, *5*, 47–58.

Duncan, L. M., H. L. Bryden, and S. A. Cunningham (2003), Friction and mixing in the Faroe Bank Channel outflow, *Oceanol. Acta*, *26*, 473–486, doi:10.1016/S0399-1784(03)00042-2.

Egbert, G. D., A. F. Bennett, and M. G. G. Foreman (1994), TOPEX/POSEIDON tides estimated using a global inverse model, *J. Geophys. Res.*, *99*, 24,821–24,852, doi:10.1029/94JC01894.

Fer, I. (2006), Scaling turbulent dissipation in an Arctic fjord, *Deep Sea Res., Part II*, *53*, 77–95, doi:10.1016/j.dsr2.2006.01.003.

Fer, I., and K. Widell (2007), Early spring turbulent mixing in an ice-covered Arctic fjord during transition to melting, *Cont. Shelf Res.*, *27*, 1980–1999, doi:10.1016/j.csr.2007.04.003.

Geyer, F., S. Østerhus, B. Hansen, and D. Quadfasel (2006), Observations of highly regular oscillations in the overflow plume downstream of the Faroe Bank Channel, *J. Geophys. Res.*, *111*, C12020, doi:10.1029/2006JC003693.

Girton, J. B., and T. B. Sanford (2003), Descent and modification of the overflow plume in the Denmark Strait, *J. Phys. Oceanogr.*, *33*, 1351–1364, doi:10.1175/1520-0485(2003)033<1351:DAMOTO>2.0.CO;2.

Girton, J. B., L. J. Pratt, D. A. Sutherland, and J. F. Price (2006), Is the Faroe Bank Channel overflow hydraulically controlled? *J. Phys. Oceanogr.*, *36*, 2340–2349, doi:10.1175/JPO2969.1.

Hansen, B., and S. Østerhus (2007), Faroe Bank Channel overflow 1995–2005, *Prog. Oceanogr.*, *75*, 817–856.

Killworth, P. D. (2001), On the rate of descent of overflows, *J. Geophys. Res.*, *106*, 22,267–22,275, doi:10.1029/2000JC000707.

Legg, S., et al. (2009), Improving oceanic overflow representation in climate models: The Gravity Current Entrainment Climate Process Team, *Bull. Am. Meteorol. Soc.*, *90*, 657–670, doi:10.1175/2008BAMS2667.1.

Mauritzen, C., J. F. Price, T. B. Sanford, and D. Torres (2005), Circulation and mixing in the Faroese Channels, *Deep Sea Res., Part I*, *52*, 883–913, doi:10.1016/j.dsr.2004.11.018.

Osborn, T. R. (1980), Estimates of the local rate of vertical diffusion from dissipation measurements, *J. Phys. Oceanogr.*, *10*, 83–89, doi:10.1175/1520-0485(1980)010<0083:EOTLRO>2.0.CO;2.

Peters, H., and H. Z. Baumert (2007), Validating a turbulence closure against estuarine microstructure measurements, *Ocean Modell.*, *19*, 183–203, doi:10.1016/j.ocemod.2007.07.002.

Peters, H., W. E. Johns, A. S. Bower, and D. M. Fratantoni (2005), Mixing and entrainment in the Red Sea outflow plume. Part I: Plume structure, *J. Phys. Oceanogr.*, *35*, 569–583, doi:10.1175/JPO2679.1.

Pratt, L. J. (2008), Critical conditions and composite Froude numbers for layered flow with transverse variations in velocity, *J. Fluid Mech.*, *605*, 281–291, doi:10.1017/S002211200800150X.

Price, J. F., et al. (1993), Mediterranean outflow and mixing dynamics, *Science*, *259*, 1277–1282, doi:10.1126/science.259.5099.1277.

Saunders, P. M. (1990), Cold outflow from the Faroe Bank Channel, *J. Phys. Oceanogr.*, *20*, 29–43, doi:10.1175/1520-0485(1990)020<0029:COFTFB>2.0.CO;2.

Saunders, P. M. (2001), The dense northern overflows, in *Ocean Circulation and Climate,* edited by G. Siedler et al., pp. 401–417, Academic, San Diego, Calif.

Shih, L. H., J. R. Koseff, G. N. Ivey, and J. H. Ferziger (2005), Parameterization of turbulent fluxes and scales using homogeneous sheared stably stratified turbulence simulations, *J. Fluid Mech.*, *525*, 193–214, doi:10.1017/S0022112004002587.

Umlauf, L. (2009), The description of mixing in stratified layers without shear in large-scale ocean models, *J. Phys. Oceanogr.*, *39*, 3032–3039, doi:10.1175/2009JPO4006.1.

Umlauf, L., and L. Arneborg (2009), Dynamics of rotating shallow gravity currents passing through a channel. Part II: Analysis, *J. Phys. Oceanogr.*, *39*, 2402–2416, doi:10.1175/2009JPO4164.1.

Umlauf, L., L. Arneborg, H. Burchard, V. Fiekas, H. U. Lass, V. Mohrholz, and H. Prandke (2007), Transverse structure of turbulence in a rotating gravity current, *Geophys. Res. Lett.*, *34*, L08601, doi:10.1029/2007GL029521.

Visbeck, M. (2002), Deep velocity profiling using lowered acoustic Doppler current profilers: Bottom track and inverse solutions, *J. Atmos. Oceanic Technol.*, *19*, 794–807, doi:10.1175/1520-0426(2002)019<0794:DVPULA>2.0.CO;2.

I. Fer, Geophysical Institute, University of Bergen, N-5007 Bergen, Norway.

K. Latarius and G. Voet, Institute of Oceanography, University of Hamburg, D-20146 Hamburg, Germany.

B. Rudels, Department of Physics, University of Helsinki, FI-00561 Helsinki, Finland.

K. S. Seim, Department of Marine Technology, Norwegian University of Science and Technology, NO-7491 Trondheim, Norway.